

## THE INFRARED MORPHOLOGY OF YOUNG STELLAR OBJECTS WITHOUT COMPANIONS: A SPECKLE INTERFEROMETRIC STUDY

L. E. DEWARF AND H. M. DYCK<sup>1</sup>

Department of Physics and Astronomy, University of Wyoming, Laramie, Wyoming 82071

Electronic mail: meldyck@corral.uwyo.edu

Received 1992 December 1; revised 1993 February 12

### ABSTRACT

One-dimensional speckle interferometric techniques are employed in the near-infrared wavelength range of 1.25 to 4.8  $\mu\text{m}$  to ascertain the morphology of eighteen young stellar objects not known to have associated companions. We find that three of these objects are resolved as core/halo distributions or are partially resolved with a high level of confidence. Five other sources probably show some structure although the confidence level is lower. The ten remaining sources either show evidence for very small angular scale structure or are unresolved with an upper limit of about 0.2 arcsec. Our results are compared to other published angular size data. A relationship between the 12 to 25  $\mu\text{m}$  spectral slope and the physical extent of the material in the near infrared is discovered and compared to simple models. We interpret this relationship as an indication that the effective scale size of circumstellar matter surrounding young stellar objects decreases with advancing age.

### 1. INTRODUCTION

To understand more fully the evolution of young stellar objects (YSO) it is imperative to know the structure of the placental clouds surrounding them. In the earliest stages of star formation, the parent cloud is extended to a few thousand Astronomical Units (AU) and a condensed core, hidden by the largely opaque cloud, grows by accretion (Larson 1973). As the core evolves to the T Tauri stage, conservation of angular momentum will create a pronounced equatorial disk of material. Theoretical models (Adams & Shu 1986; Adams *et al.* 1987, 1988) suggest that mass accretion onto this disk may produce significant flux at near- and mid-infrared wavelengths. Studies of the accretion disk and its environs are, therefore, best carried out in the infrared.

Bertout *et al.* (1988) have computed model accretion disks for objects located in the Taurus cloud. These disks have radii in the range from about 6 to 18 AU and subtend angles of less than about 0.25 arcsec as seen from the Earth. Direct measurements of angular structure are limited by atmospheric seeing to about 1 arcsec, and higher resolution data are generally available only from interferometry or lunar occultations. Unfortunately, even with the few milliarcsecond resolution possible with these latter techniques, only limited numbers of objects are surveyable owing either to brightness limits or to placement in the sky.

Some years ago, we began an observational speckle interferometry program designed to place constraints, which might be valuable for theoretical models, upon the presence of circumstellar material near the star. Presented here are the results of that study of eighteen different YSO. Employing simple models, we discuss the nature of the extended material. In addition, we have developed a

method to quantify the spurious effects of atmospheric seeing on the observed visibility data; from this we are able to assign confidence factors to our models. High angular resolution work done by other authors is added to the above set to create a catalog of the structures of these YSO.

Finally, a comparison is made between the spectral slope of the flux distribution in the mid-infrared and the near-infrared extent of the surrounding cloud. This yields an empirical relationship that we are able to explain qualitatively using existing circumstellar disk models.

### 2. PROCEDURE

#### 2.1 Observations

Observations were performed at the Mauna Kea Observatory in Hawaii using the University of Hawaii 2.2 m (UH), the NASA 3.0 m (IRTF), and the United Kingdom 3.8 m (UKIRT) telescopes between the years of 1980 and 1985. The one-dimensional speckle interferometric scans were taken between 1.25 and 4.8  $\mu\text{m}$  using the instrument, detectors, and method of acquiring the data described by Dyck & Howell (1985). A log of the observations is given in Table 1 where we list the date, telescope, coordinates, wavelength, and position angle used for the observations. In addition, cross-reference is made to the figure in which the data are displayed. The fundamental data presented here are the source visibility versus spatial frequency. These are shown in Figs. 1–3 along with models to be discussed more thoroughly in the next section.

No attempt was made to select a complete sample of sources of any particular type. Rather, sources that have been historically interesting were chosen as the highest priority.

#### 2.2 Data Reductions

The models fitted to the visibility data were primarily chosen for their mathematical simplicity. While these may

<sup>1</sup>Visiting observer; United Kingdom Infrared Telescope and Infrared Telescope Facility, operated by the University of Hawaii under contract from the National Aeronautics and Space Administration.

TABLE 1. The observing log.

Name	Date	Tele <sup>1</sup>	RA (1950) (h m s)	Dec (1950) (° ' ")	$\lambda$ ( $\mu$ m)	PA <sup>2</sup> (°)	Fig <sup>3</sup>
AFGL490	17 Nov 81	UH	03 23 41.4	+58 36 52	3.8	0	1(a)
DG Tau	2 Dec 82	IRTF	04 24 01.0	+25 59 36	3.8	0	1(b)
LkH $\alpha$ 101	8 Oct 81	UH	04 26 57.2	+35 09 56	4.8	0	3(b)
AB Aur	2 Dec 82	IRTF	04 52 34.2	+30 28 22	3.8	0	2(a)
SU Aur	17 Nov 81	UH	04 52 47.8	+30 29 19	3.8	0	3(i)
	2 Dec 82	UH			3.8	0	3(j)
BN	29-30 Dec 80	UH	05 32 49.7	-05 24 17	4.8	0	2(b)
	10 Oct 81	UH			3.8	0	2(c)
	11 Oct 81	UH			3.8	0	2(d)
	10 Nov 84	UH			2.2	0	2(e)
	30 Nov 85	UH			2.2	45	2(f)
OMC 1/IRS 2	10 Oct 81	UH	05 32 58.7	-05 11 20	3.8	0	1(c)
FU Ori	26 Nov 82	UH	05 42 38.0	+09 03 02	2.2	0	2(g)
Mon R2/IRS 2	28-30 Dec 80	UH	06 05 19.4	-06 22 25	4.8	0	3(c)
	9 Oct 81	UH			3.8	0	3(d)
	10 Oct 81	UH			3.8	0	3(e)
HD45677	8 Oct 81	UH	06 25 59.1	-13 01 12	4.8	0	2(h)
R Mon	2-4 Jan 85	UKIRT	06 36 26.0	+08 47 03	1.25	V <sup>4</sup>	1(d)
	2-4 Jan 85	UKIRT			1.6	V	1(e)
AFGL989	28 Dec 80	UH	06 38 24.9	+09 32 29	4.8	0	3(a)
W33A	20 Aug 81	UH	18 11 44.2	-17 52 59	4.8	0	1(h)
R CrA	27 May 83	UKIRT	18 58 31.6	-37 01 30	2.2	90	2(i)
	27 May 83	UKIRT			2.2	90	2(j)
	27 May 83	UKIRT			3.8	90	2(k)
	27 May 83	UKIRT			3.8	90	2(l)
	27 May 83	UKIRT			3.8	90	2(m)
	30 May 83	UH			3.8	0	2(n)
	30 May 83	UH			3.8	0	2(o)
S106/Source 3	13 Oct 81	UH	20 25 33.7	+37 12 50	2.2	0	3(h)
V1057 Cyg	13 Oct 81	UH	20 57 06.2	+44 03 46	2.2	0	3(k)
	17 Nov 81	UH			3.8	0	3(l)
S140/IRS 1	9 Oct 81	UH	22 17 41.3	+63 03 40	3.8	0	1(f)
	11 Oct 81	UH			3.8	0	1(g)
NGC7538/IRS 1	28 Dec 80	UH	23 11 36.5	+61 11 50	4.8	0	3(f)
	11 Oct 81	UH			3.8	0	3(g)

## Notes for Table 1

- <sup>1</sup> The telescope used for the observation (see text).
- <sup>2</sup> The position angle used for the observation.
- <sup>3</sup> The figure in which the visibility data are plotted.
- <sup>4</sup> V indicates that various PA have been observed.

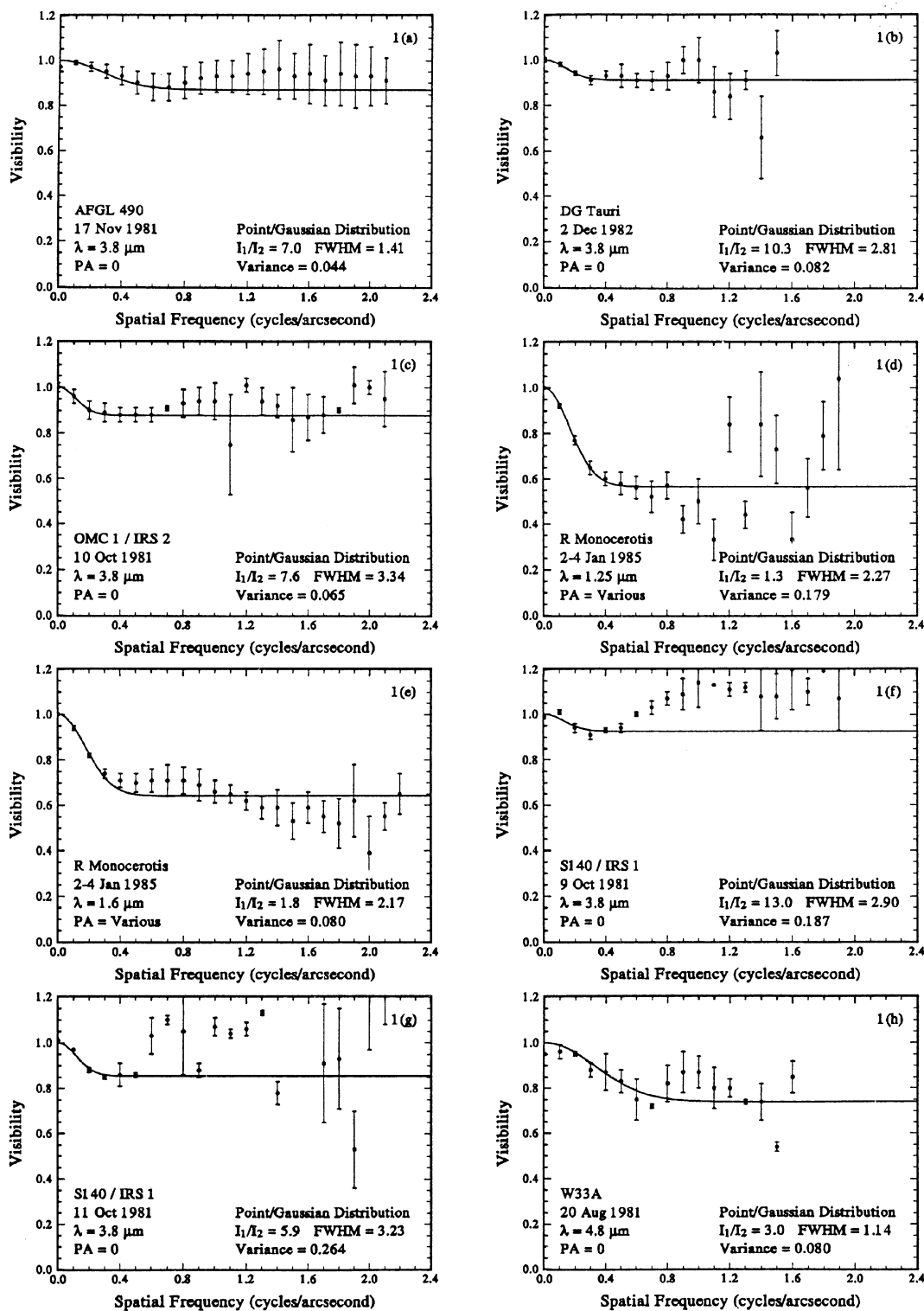


FIG. 1. Visibility data for the Point/Gaussian sources. The points are the observational data shown with  $1\sigma$  of the mean error bars computed from repeated scans of the source. The solid lines are models that are described more fully in the text. Model parameters are summarized in the figure.

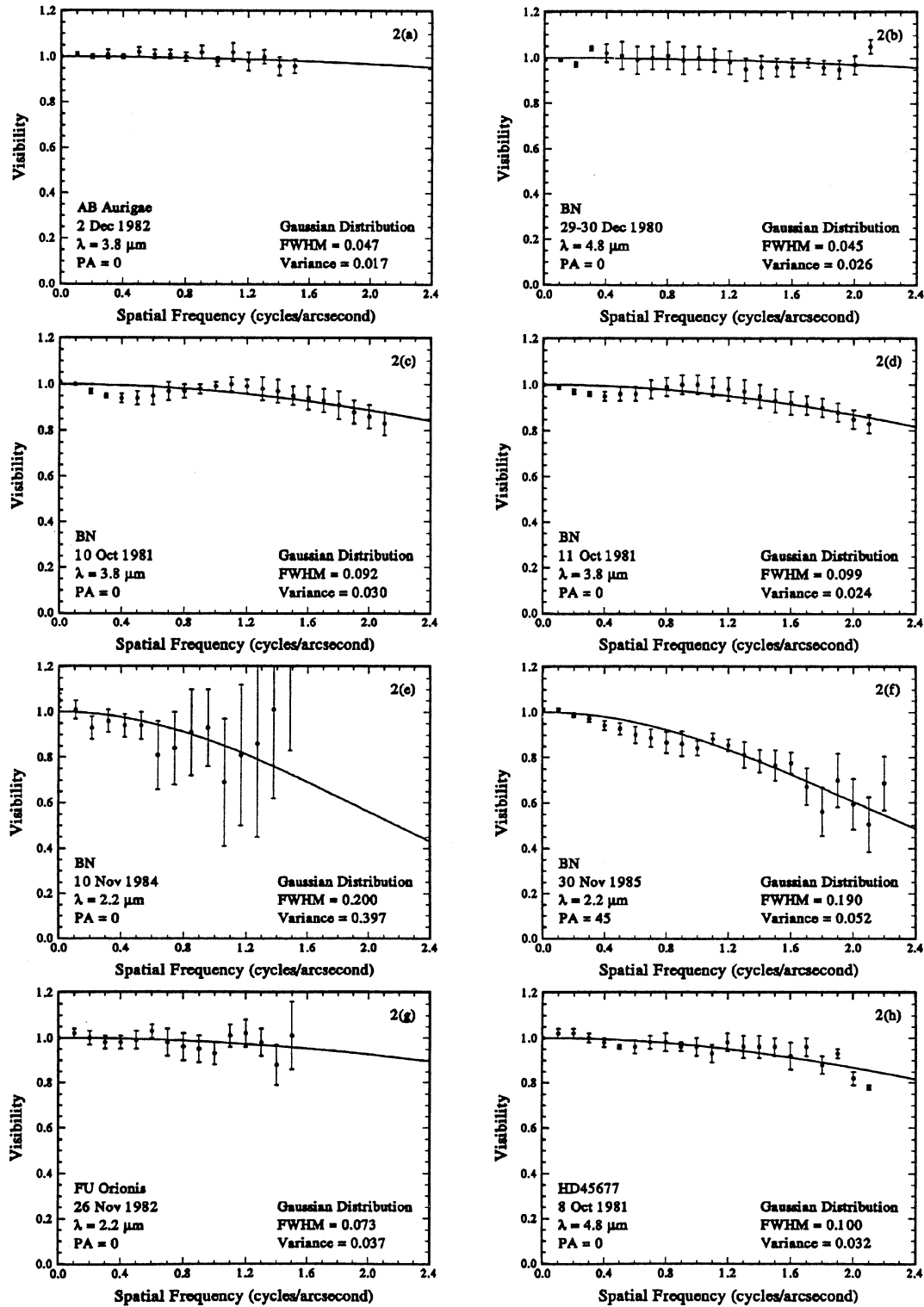


FIG. 2. Visibility data for the simple Gaussian distributions. See the caption for Fig. 1.

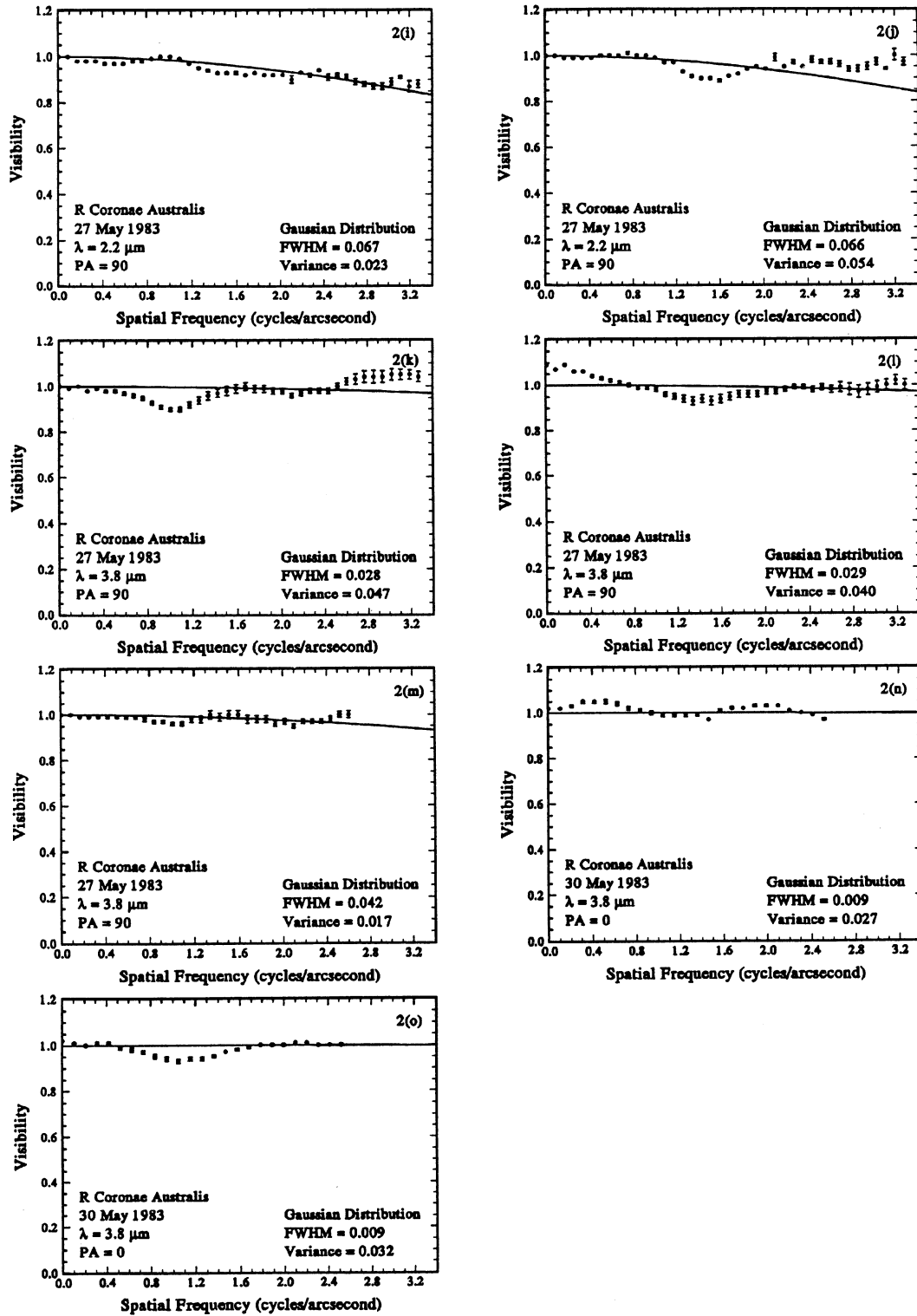


FIG. 2. (continued)

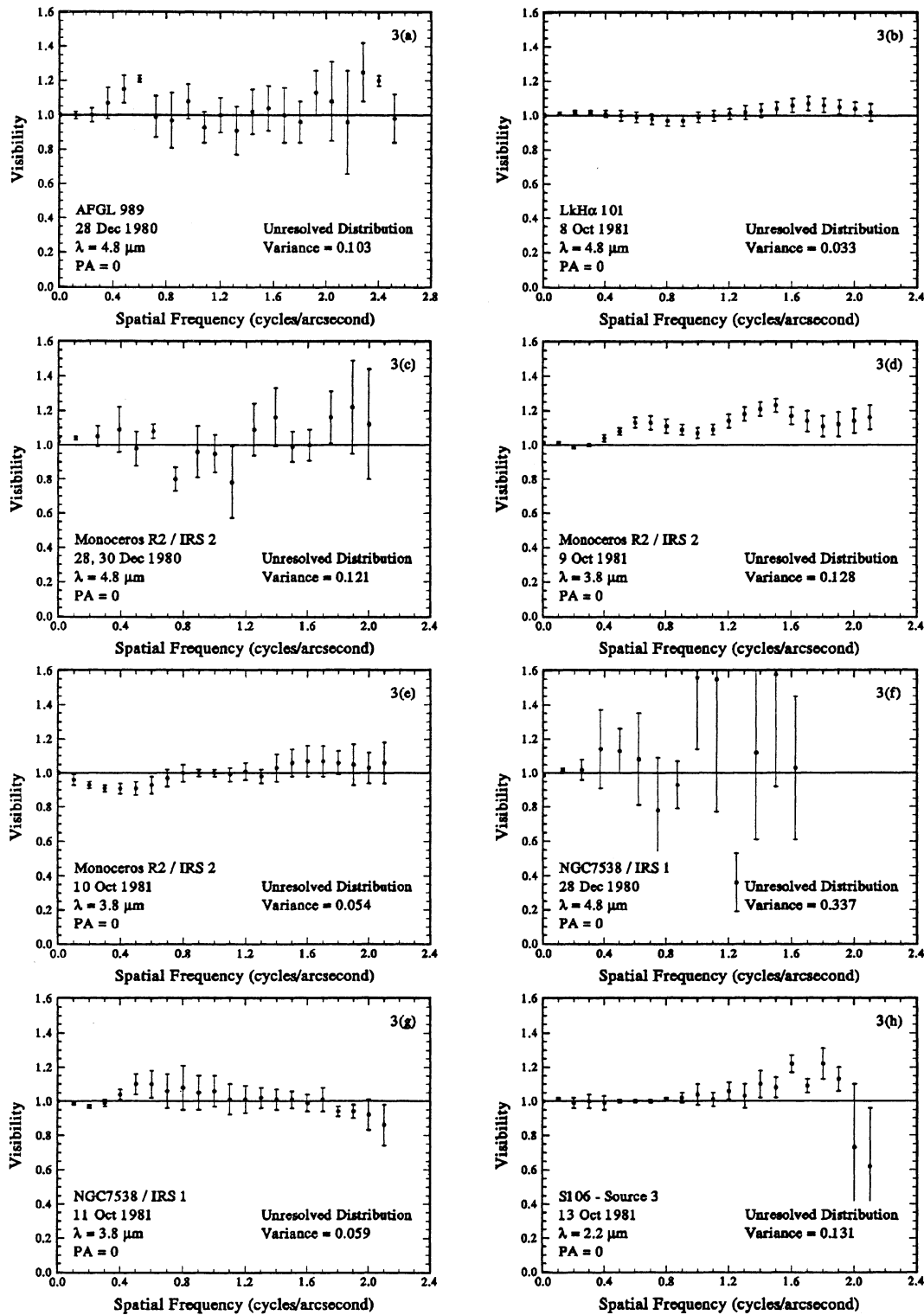


FIG. 3. Visibility data for the Unresolved sources. See the caption for Fig. 1.

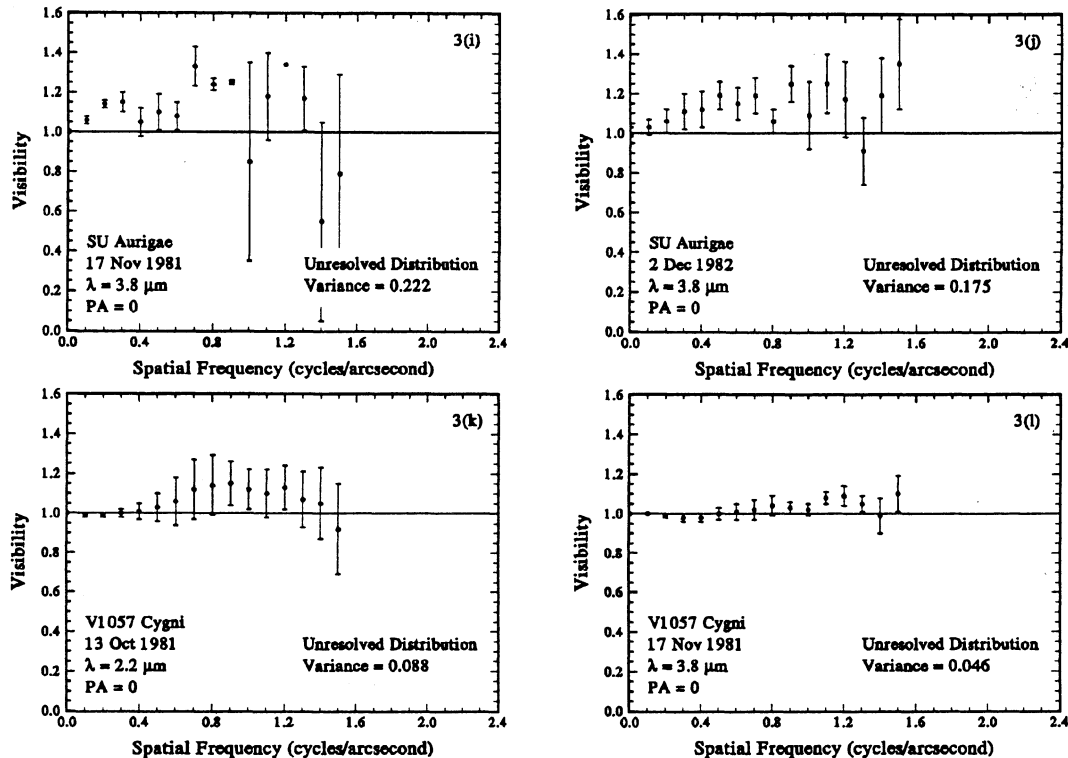


FIG. 3. (continued)

not be the most physically realistic, the computed scale sizes may generally be converted from one kind of assumed brightness distribution to any other (see, for example, Ridgway *et al.* 1986). The use of simple brightness distributions for interferometry has been discussed by Fomalont & Wright (1974) and by Beckwith *et al.* (1984). We have chosen three kinds of models detailed below.

**Point/Gaussian Distribution:** For core/halo sources

$$V(s) = V_0 + (1 - V_0) \exp\left[-\frac{2\pi^2}{8 \ln 2} \text{FWHM}^2 s^2\right],$$

where FWHM = Full Width at Half Maximum in arcsec,  $s$  is the spatial frequency in cycles/arcsec, and  $V_0$  is the ratio of point source brightness to the total brightness.

**Gaussian Distribution:** For partially resolved sources the visibility may be represented by a single Gaussian

$$V(s) = \exp\left[-\frac{2\pi^2}{8 \ln 2} \text{FWHM}^2 s^2\right],$$

where the terms were previously defined.

**Unresolved Distribution:** For a point source  $V(s) = 1$ .

For each model we generally began by minimizing the weighted variance. The weighting function was determined by the magnitude of the errors at each spatial frequency, which was obtained from the dispersion in the repeated scans. Then each model was inspected visually. If necessary, it would be further adjusted to eliminate the effects of the high spatial frequency data that appeared to be systematically in error. This procedure is equivalent to choosing,

in advance, the highest frequency data point to be trusted. A new variance, using all the data, was then calculated for the final model. Values of the variance less than about 0.1 generally imply models that fit well over the entire range of spatial frequencies measured. When the variance exceeds 0.1 there are likely to be significant departures between the model and higher spatial frequency data. Our model fits have been summarized in Table 2; the variances are given with the visibility data in Figs. 1–3. We discuss the effects of systematic errors upon the derived model parameters in the following section.

Observations of many additional sources are also available in the literature. We have summarized the work of other authors in Table 3 using the same format as our own models.

### 2.3 Systematic Errors

It may be seen in the figures that systematic errors persist in the visibility data even after correction for the telescope-atmosphere point spread function. Among the 7 sources classified as Unresolved, 10 of the 12 visibility functions rise above unity. Such behavior cannot be accounted for by any physical model and must be an artifact of the observations. It is also reasonable to expect that just as many sources that are truly unresolved will show visibilities that drop below unity (and hence, are physically plausible) as a result of the same systematic error. In order to quantify the magnitude of this effect we have developed a test using the visibilities that rise above unity. With this

test we assign a confidence factor (CF) to each model that reflects the probability that a source, which is classified as resolved, is truly resolved and not apparently resolved as a result of the systematic error.

The test rests upon the assumptions that (1) the sources that show the spurious rise in visibility are truly unresolved, and (2) there are as many unresolved sources in the sample that appear resolved as a result of the artifact. We plotted all the unresolved data together on a single visibility graph. Then, based upon assumption (2) above, we reflected the data about the  $V(s)=1$  line. This gave a distribution that was symmetric about  $V(s)=1$ . The fall-

off of visibility points below the line appeared to be normally distributed so that we were able to compute, for any arbitrary model minimum visibility, how many  $\sigma$  away from  $V(s)=1$  it lay. Using Gaussian statistics this immediately led to the probability that the test visibility belonged to the spurious population and, hence, led to a CF. In the way we have defined the CF, 100 corresponds to (asymptotic) perfect confidence; that is, there is no chance, statistically, that the measurement could be caused purely by the artifact. Conversely, when the CF=0 we have no confidence in the model. The minimum visibilities for the Point/Gaussian models came from the visibility level for

TABLE 2. The modeled distributions.

Point/Gaussian Distributions									
Name	$\lambda$	PA	Dist	$1-V_0^1$	FWHM		$\eta_{12}^2$	CF <sup>3</sup>	Refs
	( $\mu\text{m}$ )	( $^\circ$ )	(pc)	(%)	( $''$ )	(AU)		(%)	
AFGL490	3.8	0	900	13 $\pm$ 9	1.41 $\pm$ 0.69	1270	-0.59	29	5,C
DG Tau	3.8	0	140	9 $\pm$ 8	2.81 $\pm$ 0.81	393	-0.08	16	2,C
OMC 1/IRS 2	3.8	0	500	12 $\pm$ 4	3.34 $\pm$ 1.67	1670	— <sup>4</sup>	25	3
R Mon	1.25 1.65	V	800	43 $\pm$ 14 36 $\pm$ 9	2.27 $\pm$ 0.26 2.17 $\pm$ 0.26	1820 1740	-0.20	98 94	6,A
S140/IRS 1	3.8	0	910	7 $\pm$ 4 14 $\pm$ 7	2.90 $\pm$ 0.72 3.23 $\pm$ 0.28	2640 2940	-1.22	10 37	9,A
W33A	4.8	0	3700	25 $\pm$ 5	1.14 $\pm$ 0.51	4230	-2.46	74	11,A
Gaussian Distributions									
Name	$\lambda$	PA	Dist	FWHM		$\eta_{12}$	CF	Refs	
	( $\mu\text{m}$ )	( $^\circ$ )	(pc)	( $''$ )	(AU)		(%)		
AB Aur	3.8	0	140	0.047 $\pm$ 0.047	7	0.27	<1	2,C	
BN	4.8 3.8 2.2	0	500	0.045 $\pm$ 0.040 0.092 $\pm$ 0.033 0.099 $\pm$ 0.025 0.200 $\pm$ 0.190 0.190 $\pm$ 0.034	23 46 50 100 95	0.19	2 28 36 86 99	3,B	
FU Ori	2.2	0	480	0.073 $\pm$ 0.073	35	-0.16	4	3,D	
HD45677	4.8	0	1000	0.100 $\pm$ 0.020	100	1.03	37	13,A	
R CrA	2.2 3.8	90	130	0.067 $\pm$ 0.001 0.066 $\pm$ 0.001 0.028 $\pm$ 0.018 0.029 $\pm$ 0.020 0.042 $\pm$ 0.010 0.009 $\pm$ 0.001 0.009 $\pm$ 0.001	9 9 4 4 5 1 1	0.06	42 40 2 2 4 <1 <1	12,A	

TABLE 2. (continued)

## Unresolved Distributions

Name	$\lambda$	PA	Dist	FWHM	$\eta_{12}$	Refs
	( $\mu\text{m}$ )	( $^\circ$ )	(pc)	(AU)		
AFGL989	4.8	0	800	<160	-0.46	4, B
LkH $\alpha$ 101	4.8	0	800	<160	1.09	8, A
Mon R2/IRS 2	4.8 3.8	0	950	<190 <190 <190	$\approx 1^5$	14, B
NGC7538/IRS 1	4.8 3.8	0	3500	<700 <700	-1.63	10, B
S106/Source 3	2.2	0	900	<180	$\approx -2^5$	7, E
SU Aur	3.8	0	140	< 28 < 28	-0.65	2, F
V1057 Cyg	2.2 3.8	0	700	<140 <140	0.03	1, A

## Notes for Table 2

- <sup>1</sup> The fractional flux contained in the extended component relative to the total flux.  
<sup>2</sup> The spectral slope between 12  $\mu\text{m}$  and 25  $\mu\text{m}$ .  
<sup>3</sup> The model confidence factor, described in the text.  
<sup>4</sup> No data are available.  
<sup>5</sup> Poorly determined value.

## References for Table 2

- (1) Chavarría-K. (1981); (2) Elias (1978);  
(3) Genzel *et al.* (1981); (4) Harvey *et al.* (1977);  
(5) Harvey *et al.* (1979a); (6) Harvey *et al.* (1979b);  
(7) Harvey *et al.* (1982); (8) Herbig (1971);  
(9) Howell *et al.* (1981); (10) Israel (1977);  
(11) Jaffe *et al.* (1982); (12) Marraco & Rydgren (1981);  
(13) Swings & Allen (1971); (14) Thronson *et al.* (1980).  
(A) PSC; (B) Gezari *et al.* (1987); (C) Clark (1991);  
(D) Cohen *et al.* (1989); (E) Herter *et al.* (1982);  
(F) Strom *et al.* (1989).

the point source; and for the single Gaussian from the model visibility at the highest spatial frequency where we obtained data.

## 3. DISCUSSION

## 3.1 The Spectral Slope Relation

The origin of the infrared flux emitted by a YSO has been the subject of investigation for nearly two decades. The earlier interpretative efforts, for example Rowan-Robinson (1979, 1980), dealt mainly with the most luminous of the YSO. In these cases the infrared radiation was thought to be mainly stellar light reprocessed in an exten-

sive, dusty circumstellar shell. More recently, attention has been focused upon the lower luminosity YSO with the recognition that accretion disks near the stellar photosphere play an important role in producing direct infrared radiation. In the models of Bertout *et al.* (1988), the entire flux spectrum of many T Tauri stars is well reproduced by the star and accretion disk. However, for some of the stars, notably the ones with the reddest mid-infrared spectra, their models predict an order of magnitude lower level of flux at  $\lambda > 10 \mu\text{m}$  than is observed. Although modified accretion disk schemes have been suggested to account for this discrepancy, it seems reasonable that the whole spec-

TABLE 3. The distributions from the literature.

Point/Gaussian Distributions								
Name	$\lambda$	PA	Dist	$1-V_0$	FWHM		$\eta_{12}$	Refs
	( $\mu\text{m}$ )	( $^\circ$ )	(pc)	(%)	( $''$ )	(AU)		
AFGL490	1.62	0	900	32	1.05	950	-0.59	4,C
		90		27	1.26	1130		
	2.28	0	18	1.13	1020			
		90	14	1.34	1210			
	3.7	0	8	1.11	1000			
		90	14	1.24	1120			
DG Tau	1.25	45	140	9	0.64	90	-0.08	7,C
	1.65			14	0.85	119		
	2.2	0	3	0.75	105			
	1.25	135	6	0.90	126			
	1.65		10	0.76	106			
Elias 21	3.6	V	160	34	3.0	480	-0.79	12,B
Elias 29	3.6	V	160	10	3.5	560	-0.33	13,F
HL Tau	2.2	0	140	30	1.24	174	-0.79	1,E
		90		27	2.07	290		
	3.8	0	9	0.26	36			
		90	9	1.05	147			
LkH $\alpha$ 198	1.25	V	600	26	0.70	420	0.20	8,B
				20	2.20	1320		
	1.62		19	0.50	300			
			23	1.65	990			
	2.28		6	0.20	120			
			13	1.40	840			
		6	0.17	102				
		4	1.30	780				
LkH $\alpha$ 233	1.62	V	880	33	0.51	449	-1.23	9,B
				17	2.2	1940		
	2.28		8	0.75	660			
			12	1.7	1500			
R Mon	2.2	0	800	14	1.62	1300	-0.20	1,A
		90		13	1.61	1290		
	3.8	0	9	0.57	456			
		90	5	1.42	1140			
S140/IRS 1	4.8	0	910	13	2.70	2460	-1.22	2,A
V376 Cas	1.62	V	600	13	0.49	294	—	8
				18	2.28	1370		
	2.28		5	0.42	252			
			7	1.94	1160			
			4	0.53	318			
V380 Ori	2.2	0	460	11	0.40	184	1.15	1,C
		90		<	0.20	<		

TABLE 3. (continued)

## Gaussian Distributions

Name	$\lambda$	PA	Dist	FWHM	$\eta_{12}$	Refs
	( $\mu\text{m}$ )	( $^{\circ}$ )	(pc)	( $''$ )	(AU)	
BN	3.5	40	500	0.047	24	0.19 3,B
				0.059	30	
	4.8	0		0.047	24	2
MWC349	2.2	0	1200	0.038	46	2.21 6,B
	3.8	90		0.085	102	
NGC2024 #2	4.64	90	500	0.077	39	1.76 5,D
YLW 16A	2.2	325	160	0.3	50	-1.56 11,G

## Unresolved Distributions

Name	$\lambda$	PA	Dist	FWHM	$\eta_{12}$	Refs
	( $\mu\text{m}$ )	( $^{\circ}$ )	(pc)	(AU)		
AFGL2591	4.6	33	1500	$\leq 126$	-0.38	10,C
	3.5	—	1500	< 62		3

## References for Table 3

- (1) Beckwith *et al.* (1984); (2) Dyck & Howell (1982);  
 (3) Foy *et al.* (1979); (4) Haas *et al.* (1992);  
 (5) Jiang *et al.* (1984); (6) Leinert (1986);  
 (7) Leinert *et al.* (1991a); (8) Leinert *et al.* (1991b);  
 (9) Leinert *et al.* (1992); (10) Mariotti *et al.* (1983);  
 (11) Simon *et al.* (1987); (12) Zinnecker *et al.* (1987a);  
 (13) Zinnecker *et al.* (1987b).
- (A) PSC; (B) Gezari *et al.* (1987); (C) Clark (1991);  
 (D) Grasdalen (1974); (E) Strom *et al.* (1989);  
 (F) Wilking *et al.* (1989); (G) Young *et al.* (1986).

trum must generally be a combination of the stellar atmosphere, an accretion disk, and some remaining more extended material that reprocesses deeper radiation. This possibility was mentioned briefly by Bertout *et al.* (1988). Observationally, this problem has been addressed by Leinert *et al.* (1991a) in their discussion of the disk properties of DG Tau. They noted that the expected accretion disk for that star was significantly smaller in size than the halo of material that they measured. They suggested that the near-infrared speckle interferometry was, in fact, measuring scattered radiation that originated in a deeper source. In the discussion that follows we adopt their simple interpretation of the hierarchy of dusty material surrounding the central star.

Weintraub (1990) has shown that YSO with dusty halos tend to have 12–25  $\mu\text{m}$  *IRAS* colors within a relatively narrow range of values. If the halos are heated by radiation from the stellar photosphere and the accretion disk, then to first order, one expects to observe a correlation between the size of a dust cloud and its color: The temperature will generally be cooler in the more extensive clouds. Thus one expects that the larger linear cloud sizes will be associated with the spectrally redder sources. We make the assumption that larger clouds will also appear larger in scattered light measured by speckle interferometry. Therefore, although they arise from very different physical mechanisms in different regions, there ought to be a relation between the source redness in the thermal infrared and our mea-

sured sizes in the near infrared. In order to investigate the possibility of a relationship between the size and color of a cloud we used the spectral slope as defined by Adams *et al.* (1987)

$$\eta = \frac{d \log(\nu F_\nu)}{d \log(\nu)},$$

where  $F_\nu$  is the flux density per unit frequency at frequency  $\nu$ .

The region between 12 and 25  $\mu\text{m}$  was chosen because the accretion disk models for T Tauri stars suggest that this radiation may be significantly reprocessed. Furthermore the *IRAS Point Source Catalog* (Joint *IRAS* Science Working Group 1988; hereafter PSC) contains the relevant fluxes for many of our sources. In this range we may approximate

$$\eta_{12} \approx \frac{\log\left(\frac{\nu_{12} F_{12}}{\nu_{25} F_{25}}\right)}{\log\left(\frac{\nu_{12}}{\nu_{25}}\right)},$$

where the subscripts refer to the wavelengths 12  $\mu\text{m}$  and 25  $\mu\text{m}$ . The more negative spectral slopes correspond to redder objects.

In choosing fluxes we gave first preference to high angular resolution ground-based data in order to avoid source confusion. Second preference was given to data in the *IRAS* catalog that may, in some cases, be contaminated by nearby sources owing to the large field of view. For some sources no data at 12 or 25  $\mu\text{m}$  was available and it was necessary to infer fluxes either by interpolating a smooth curve through data at bracketing wavelengths or by extrapolating from observations at 20  $\mu\text{m}$  and shorter wavelengths. The spectral slopes for the sources are given in Tables 2 and 3. The average rms dispersion in the calculation of the spectral slope is found to be approximately  $\pm 0.1$  for the entire sample, determined when more than one of the above methods for acquiring the fluxes was available for a given source.

In order to make use of the largest quantity of data, we have considered all angular diameter measurements together. When diameters were available at more than one wavelength, we averaged the values. When only one value was available, we took that one. This method of data selection yields a diameter at an average wavelength near 3.5  $\mu\text{m}$  for the entire sample of sources listed in the tables. Such averaging will produce inevitable scatter. Many sources exhibit a decrease of halo diameter with increasing wavelength. Examples of this kind of source are BN, HL Tau, and R Mon. Some other sources appear to have roughly constant angular sizes with wavelength. An example of this kind of source is DG Tau. We estimate that our averaging will produce a spread in the diameters of less than a factor of 2. As we will see this is considerably less than the observed spread of diameters at a given spectral slope.

We have plotted the results of this study in Fig. 4 as spectral slope versus linear diameter. For our sources we

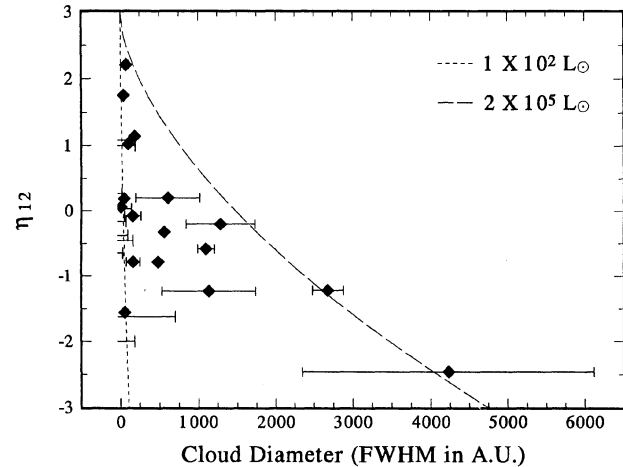


FIG. 4. A plot of the 12–25  $\mu\text{m}$  spectral slope vs the linear diameter of the remnant material surrounding the YSO. The points are plotted with dispersion bars that are estimates of their possible range of values in linear diameter, while upper limits for the cloud extents are shown as left-pointing tic marks. The average rms dispersion in the spectral slope is represented by the height of the diamond. The two lines are the simple models described in the text: The long-dashed line refers to a central source luminosity of  $2 \times 10^5 L_\odot$  and the short-dashed line refers to a central source luminosity of  $100 L_\odot$ .

have generally taken the linear diameter inferred from the simple models. In cases where the determination was statistically uncertain or the CF were very low, we have taken upper limits based upon the observing statistics. For sources classed as unresolved we have taken 0.2 arcsec as the upper limit, based upon our consideration of the CF.

The plot shows that sources that have diameters larger than about 1000 AU are redder than  $\eta_{12} \approx 0$  but that sources that are bluer than  $\eta_{12} \approx 0$  have diameters less than about 500 AU. We can quantify this by considering the average sizes for sources in the two color categories. Sources with  $\eta_{12} \geq 0$  have an average size of about 150 AU with only one source larger than 200 AU. Sources with  $\eta_{12} < 0$  have an average size of about 1200 AU. Even with the two largest sources (S140/IRS1 and W33A) removed from the latter sample, the group has an average size of about 600 AU, roughly four times the average size of the bluer group. Our results may be qualitatively understood in terms of the model predictions of Adams *et al.* (1987) who postulated an evolutionary sequence ranging from negative slopes for protostars through near-zero slopes for T Tauri stars to positive slopes for pre-main-sequence (PMS) stars that have largely cleared their remnant material. Our relation shown in Fig. 4 would have the following interpretation: Sources with larger diameter circumstellar halos are in earlier stages of evolution while sources with bluer colors are in later stages. As a source ages, it would tend to move from the lower right to the upper left in the figure.

One interesting problem is the spread of diameters seen at a given value of the spectral slope. As we have previously discussed, part of this scatter is caused by combining data from various wavelengths. An estimate of this source

of scatter has been given as an rms “dispersion bar” for the resolved source diameter when the point plotted was taken from a range of values at different wavelengths. It is evident that this does not account for the magnitude of the scatter observed. A second potential source of dispersion is the geometrical aspect resulting from the position of the observer with respect to a nonspherical source. Adams *et al.* (1988) have shown that, for circumstellar disk geometry, a high inclination angle (i.e., the disk viewed nearly edge-on) will result in significant reddening. Undoubtedly some of the observed scatter may result from this geometrical effect. However, owing to the relative infrequency of edge-on disks to be expected if the distribution is random, we believe that geometrical reddening will be a minor effect.

It should be noted parenthetically that HL Tauri is one *potential* candidate for a circumstellar disk viewed nearly edge-on. From their millimeter observations of the  $^{13}\text{CO}$  emission, Sargent & Beckwith (1987, 1991) found a long, narrow distribution of material with an aspect ratio of about 6, implying a disk inclination of order  $80^\circ$ . If the circumstellar material is actually contained in a disk, this would lend support to Cohen's (1983) suggestion that the disk must be seen nearly edge-on. Conversely, observations in the near-infrared by Beckwith *et al.* (1984, 1989) show the source to be nearly symmetric and they argue that it is feasible that this scattering material is not directly associated with the disk, but is instead particles accreting onto the disk and star.

A more likely cause of the dispersion in Fig. 4 is the source luminosity differences. The plot includes sources ranging in luminosity from about  $10 L_\odot$  for the T Tauri stars up to a few times  $10^5 L_\odot$  for the brightest molecular cloud sources. For a given linear sized circumstellar halo a less luminous source will produce less dust heating than will a more luminous source. Therefore, the less luminous source will appear redder than the more luminous one. In order to quantify this notion, we consider a simple model for which the circumstellar halo has some finite size that decreases with the advancing age of the YSO. Further, we assume that the dust temperature at the cloud boundary may be determined via the optically thin approximation for small black spheres and that the YSO luminosity is constant with advancing age at this evolutionary stage. Thus the temperature at the cloud boundary will be

$$T_b = 280 \left[ \frac{L_{\text{YSO}}/L_\odot}{R_c^2} \right]^{1/4} \text{ K},$$

where  $R_c$  is the radius of the cloud in AU and  $L_{\text{YSO}}$  is the luminosity of the underlying YSO. The assumptions allow us to scale the cloud boundary temperature inversely as the square root of the radius and, therefore, compute a cloud's spectral slope as a function of its size.

Two extreme cases have been shown plotted in Fig. 4. The long-dashed line represents a central source luminosity of  $2 \times 10^5 L_\odot$ , while the short-dashed line corresponds to  $100 L_\odot$ . The effect of decreasing the luminosity for a fixed cloud diameter is to move the source downward in the plot, as expected. It is noteworthy that all the sources are essen-

tially contained between the two extremes shown, in rough agreement with the range of observed luminosities (although the models at low luminosities are compressed, so that discrimination at that level is not great). In particular, no sources lie substantially above and to the right of the upper luminosity limit considered. This is true in spite of the model being greatly simplified.

### 3.2 The Individual Sources

From an inspection of Table 2 we conclude that three sources are resolved with a high degree of confidence: R Mon and W33A are core/halo and BN is a simple Gaussian. Five other sources (AFGL490, OMC1/IRS2, S140/IRS1, HD45677 and R CrA) may be resolved although the confidence level is lower. In the following paragraphs we comment on some of our sources and compare the measurements to other published observations whenever possible.

**R Monocerotis:** This object was first reported by Beckwith *et al.* (1984) who observed structure of order 1.5 arcsec at 2.2 and  $3.8 \mu\text{m}$  at  $\text{PA}=0^\circ$  and  $90^\circ$ . Our observations at 1.25 and  $1.65 \mu\text{m}$  averaged over four PA reveal a size of roughly 2 arcsec for the material near the star. We have inspected our individual visibility curves at each PA and concluded that no significant difference occurs within the measurement errors. We note that the relative contribution of the flux from the Gaussian halo to the total source flux decreases smoothly with increasing wavelength from 43% at  $1.25 \mu\text{m}$  to approximately 6% at  $3.8 \mu\text{m}$ . The fractional contribution can be adequately represented by a simple power law varying as  $\lambda^{-1.8}$ . For circumstellar matter illuminated by scattered starlight this behavior implies the presence of scattering particles smaller than the wavelength.

**R Coronae Australis:** This object is similar in appearance to R Mon; both have prominent associated conical nebulae visible at optical wavelengths. However, R CrA does not show the same small scale spatial structure near the star as R Mon. Our observations at  $3.8 \mu\text{m}$  and two position angles are consistent with the source being unresolved. The formal fit to the data at  $2.2 \mu\text{m}$  yields a source diameter of order 9 AU (there is roughly a 60% chance that the visibilities could have been affected by an observational artifact). It is interesting to note in this context that Bibo *et al.* (1992) have argued independently that the dust that produces the near-infrared flux must lie within a radius of about 2 AU of the star.

**AFGL490:** Our model reported in Table 2 is assigned a low CF. However, recent observations by Haas *et al.* (1992) yield models in close agreement with ours, showing that our measurements were not affected by artifacts.

**DG Tauri:** Our measurements show a low surface brightness halo of order 3 arcsec in size at  $3.8 \mu\text{m}$  although the model has a very low CF. Beckwith *et al.* (1984) reported only an upper limit at  $3.8 \mu\text{m}$  in a direction orthogonal to ours. However, these determinations are inconsistent with the recent model results of Leinert *et al.* (1991a) who report a halo of order  $3/4$  arcsec size corresponding

roughly to 100 AU. The models of Bertout *et al.* (1988) assume an accretion disk with a diameter of 28 AU, about a factor of 4 smaller than the size measured by Leinert *et al.* (1991a).

**FU Orionis:** Our observations show that this star is probably unresolved (our model value has a near-zero CF). If we take the model FWHM at face value then the inferred linear structure would have a diameter of order 35 AU at a source distance of 480 pc; the upper limit is about three times this value. The models proposed by Kenyon *et al.* (1988) suggest that the 3.5  $\mu\text{m}$  flux from the accretion disk arises predominantly in a region of about 1.1 AU diameter, which is more than two orders of magnitude smaller than our upper limit. This hierarchy is consistent with our assumed model.

**V1057 Cygni:** This second FU Ori class variable star is also unresolved at 2.2 and 3.8  $\mu\text{m}$ . An angular upper limit of 0.2 arcsec leads to a linear upper limit of 140 AU, if the distance is assumed to be 700 pc. The Kenyon *et al.* (1988) model predicts a 3.5  $\mu\text{m}$  diameter of about 1.2 AU, two orders of magnitude smaller than our upper limit.

**S140/IRS1:** Our measurements suggest a core/halo structure at 3.8  $\mu\text{m}$  with a 3 arcsec halo diameter, although the assigned CF are low. The measurement reported by Dyck & Howell (1982) yields approximately the same size at 4.8  $\mu\text{m}$ . More careful observations of this source will be needed to confirm the halo structure.

**BN:** Our measurements of this source reveal a decrease of size between 2.2  $\mu\text{m}$  and longer wavelengths although the models at 3.8 and 4.8  $\mu\text{m}$  are assigned low CF. These

results agree with those obtained by Foy *et al.* (1979), Howell (1980), and Dyck & Howell (1982).

#### 4. CONCLUSION

We have presented new infrared speckle interferometry for 18 YSO not known to have associated companions. None of the sample was found to be multiple. Forty-five percent of our sample appear to be resolved and the remainder marginally resolved or unresolved. In addition, we have summarized other results from the literature for sources without companions. When we compare the linear sizes with mid-infrared spectral slopes we find a relationship that suggests that the physically larger sources are generally the more red ones. Conversely, the bluest sources appear to have little or no evidence for extensive circumstellar structure. We interpret this result as an indication that the "effective" size of the circumstellar remnant left over from the star-formation process decreases with advancing age of the YSO. The observations appear to agree with the recent evolutionary scenario proposed by Adams *et al.* (1987).

The authors would like to acknowledge the assistance of R. R. Howell at the telescope and for valuable conversations. L.E.D. also would like to thank T. N. Titus and D. R. Klassen for many useful discussions. We thank NSF for partial support through Grant Nos. AST-8208793 and AST-9021181.

#### REFERENCES

- Adams, F. C., Lada, C. J., & Shu, F. H. 1987, *ApJ*, 312, 788  
 Adams, F. C., Lada, C. J., & Shu, F. H. 1988, *ApJ*, 326, 865  
 Adams, F. C., & Shu, F. H. 1986, *ApJ*, 308, 836  
 Beckwith, S., Zuckerman, B., Skrutskie, M. F., & Dyck, H. M. 1984, *ApJ*, 287, 793  
 Beckwith, S. V. W., Sargent, A. I., Koresko, C. D., & Weintraub, D. A. 1989, *ApJ*, 343, 393  
 Bertout, C., Basri, G., & Bouvier, J. 1988, *ApJ*, 330, 250  
 Bibo, E. A., The, P. S., & Dawanas, D. N. 1992, *A&A*, 260, 293  
 Chavarría-K., C. 1981, *A&A*, 101, 105  
 Clark, F. O. 1991, *ApJS*, 75, 611  
 Cohen, M. 1983, *ApJ*, 270, L69  
 Cohen, M., Emerson, J. P., & Beichman, C. A. 1989, *ApJ*, 339, 455  
 Dyck, H. M., & Howell, R. R. 1982, *AJ*, 87, 400  
 Dyck, H. M., & Howell, R. R. 1985, *Proc. SPIE*, 556, 274  
 Elias, J. 1978, *ApJ*, 224, 857  
 Fomalont, E. B., & Wright, M. C. H. 1974, in *Galactic and Extragalactic Radio Astronomy*, edited by G. L. Vershuur and K. I. Kellerman (Springer, New York), Chap. 10  
 Foy, R., Chelli, A., Sibille, F., & Léna, P. 1979, *A&A*, 79, L5  
 Genzel, R., Reid, M. J., Moran, J. M., & Downes, D. 1981, *ApJ*, 244, 884  
 Gezari, D. Y., Schmitz, M., & Mead, J. M. 1987, *Catalog of Infrared Observations*, NASA Reference Publication 1196, second edition  
 Grasdalen, G. L. 1974, *ApJ*, 193, 373  
 Haas, M., Leinert, Ch., & Lenzen, R. 1992, *A&A*, 261, 130  
 Harvey, P. M., Campbell, M., & Hoffmann, W. F. 1977, *ApJ*, 215, 151  
 Harvey, P. M., Campbell, M., Hoffmann, W. F., Thronson, H. A., & Gatley, I. 1979a, *ApJ*, 229, 990  
 Harvey, P. M., Thronson, H. A., & Gatley, I. 1979b, *ApJ*, 231, 115  
 Harvey, P. M., Gatley, I., Thronson, H. A., & Werner, M. W. 1982, *ApJ*, 258, 568  
 Herbig, G. H. 1971, *ApJ*, 169, 537  
 Herter, T., Helfer, H. L., Pipher, J. L., Briotta, D. A., Forrest, W. J., Houk, J. R., Rudy, R. J., & Wilner, S. P. 1982, *ApJ*, 262, 153  
 Howell, R. R. 1980, Ph.D. thesis, University of Arizona  
 Howell, R. R., McCarthy, D. W., & Low, F. J. 1981, *ApJ*, 251, L21  
 Israel, F. P. 1977, *A&A*, 59, 27  
 Jaffe, D. T., Stier, M. T., & Fazio, G. G. 1982, *ApJ*, 252, 601  
 Jiang, D. R., Perrier, C., & Léna, P. 1984, *A&A*, 135, 249  
 Joint IRAS Science Working Group 1988, *The Point Source Catalog, Version 2* (U.S. GPO, Washington, DC)  
 Kenyon, S. J., Hartmann, L., & Hewett, R. 1988, *ApJ*, 325, 231  
 Larson, R. B. 1973, *ARA&A*, 11, 219  
 Leinert, Ch. 1986, *A&A*, 155, L6  
 Leinert, Ch., Haas, M., Richichi, A., Zinnecker, H., & Mundt, R., 1991a, *A&A*, 250, 407  
 Leinert, Ch., Haas, M., & Lenzen, R. 1991b, *A&A*, 246, 180  
 Leinert, Ch., Haas, M., & Weitzel, N. 1992, *A&A* (in press)  
 Marraco, H. G., & Rydgren, A. E. 1981, *AJ*, 86, 62  
 Mariotti, J. M., Chelli, A., Foy, R., Léna, P., Sibille, F., & Tchountonov, G. 1983, *A&A*, 120, 237  
 Ridgway, S. T., Joyce, R. R., Connors, D., Pipher, J. L., & Dainty, C. 1986, *ApJ*, 302, 662  
 Rowan-Robinson, M. 1979, *ApJ*, 234, 111  
 Rowan-Robinson, M. 1980, *ApJS*, 44, 403  
 Sargent, A. I., & Beckwith, S. V. W. 1987, *ApJ*, 323, 294  
 Sargent, A. I., & Beckwith, S. V. W. T. 1991, *ApJ*, 382, L31  
 Simon, M., Howell, R. R., Longmore, A. J., Wilking, B. A., Peterson, D. M., & Chen, W.-P. 1987, *ApJ*, 320, 344

- Strom, K. M., Strom, S. E., Edwards, S., Cabrit, S. & Skrutskie, M. F. 1989, AJ, 97, 1451  
Swings, J. P., & Allen, D. A. 1971, ApJ, 167, L41  
Thronson, H. A., Gatley, I., Harvey, P. M., Sellgren, K., & Werner, M. W. 1980, ApJ, 237, 66  
Weintraub, D. A. 1990, ApJS, 74, 575
- Wilking, B. A., Lada, C. J., & Young, E. T., 1989, ApJ, 340, 823  
Young, E. T., Lada, C. J., & Wilking, B. A., 1986, ApJ, 304, L45  
Zinnecker, H., Chelli, A., & Perrier, C. 1987a, in Star Forming Regions, edited by M. Peimbert and J. Jugaku (Reidel, Dordrecht), p. 71  
Zinnecker, H., Perrier, C., & Chelli, A. 1987b, in Circumstellar Matter, edited by I. Appenzeller and C. Jordan (Reidel, Dordrecht), p. 65